Available online at www.sciencedirect.com

ScienceDirect

journal homepage: www.elsevier.com/locate/he

Elucidating reaction equations of TiF_x ($x = 4,3,2$) catalysts for hydrogen storage applications

R. Mariyal Jebasty, R. Vidya *

Department of Medical Physics, Anna University, Sardar Patel Road, Guindy, Chennai-600025, India

HIGHLIGHTS

- For the first time, H_2 dissociation energy and reaction equations are predicted.
- Potential catalysts are identified to make metal hydrides meet targets of DoE _2020.
- 4.6 wt% H_2 released with <40 kJ/mol energy when TiF_4 & TiF_3 are added to $Mg(BH_4)_2$.
- Bond strength analysis explains the catalytic activity of the titanium fluorides.

GRAPHICAL ABSTRACT

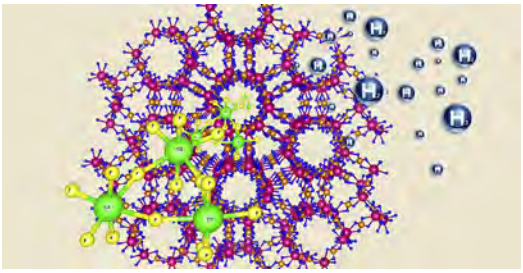

ARTICLE INFO

Article history:
Received 19 September 2019
Received in revised form
22 November 2019
Accepted 25 November 2019
Available online xxx

Keywords:
TiF catalyst
Reaction energetics
Density functional theory
Solid metal hydrides

ABSTRACT

In the never ending quest for clean energy, storing chemical energy in the form of hydrogen molecules in solid state materials is a premier choice. The release of H_2 from the H-storage (absorbent) material is hindered by the on-set of reaction mechanism which depends on the energy barrier. In a search for efficient onset (re)hydrogenation temperature, stimuli like catalysts have drawn more attention in the hydrogen fuel economy. It is laborious to down-select the aspirant candidates by screening their material properties and the thermochemical energy which are required for bond breaking. An understanding on perceptible energies involved in breaking/creating bonds has been obtained using the novel "Interface Reaction tool". To enlighten the underpinning catalytic reaction mechanism to the absorbent, the energetics of interactions between the catalyst and the solid metal hydrides have been derived. For this test study, a leading catalyst TiF_x ($x = 4,3$, and 2) has been added to the well-studied high gravimetric metal hydrides such as MgH_2, $Mg(BH_4)_2$, and $Mg(AlH_4)_2$. The reaction equation at ambient condition has been validated using the total energies from Kohn-Sham density-functional-theory, and the outcome emphasizes the importance of bonding analysis. Hence, we exemplified the bonding states of all the Ti–F derivatives namely TiF_4, TiF_3 and TiF_2 in an effort to elucidate the role of fluorine for the onset of catalytic reaction. Our detailed analysis of reaction pathways indicate the vitality of TiF_4 as an additive before and after the H_2 release. Our work pioneers the study on often overlooked reaction possibilities at ambient condition. The calculated reaction energy of less than 40 kJ/mol and 4.64 wt % of H_2 release for TiF_4 and TiF_3

* *Corresponding author.*
E-mail address: vidyar@annauniv.edu (R. Vidya).

https://doi.org/10.1016/j.ijhydene.2019.11.187

Please cite this article as: Jebasty RM, Vidya R, Elucidating reaction equations of TiF_x ($x = 4,3,2$) catalysts for hydrogen storage applications, International Journal of Hydrogen Energy, https://doi.org/10.1016/j.ijhydene.2019.11.187

underscores their catalytic activity and meet the system targets set by DoE for the year 2020. This work presents "significant disclosures" on the hydrogen decomposition mechanism and provides a platform for the feasibility study of a new material. This proposes an innovative methodology for predicting the suitability of a new material for efficient production of H_2 fuel.

Introduction

Solid state hydrogen storage materials play a vital role in hydrogen fuel economy. In order to achieve the potential targets set by Department of Energy (DoE) for 2020 [1], research communities are focusing on the fundamental understanding of reaction thermodynamics instead of searching for a new material. The goals set by DoE is reached in $NaAlH_4$ with maximum 5.6 wt% of H_2 released in total through a two-step desorption reaction. However, only 3.7 wt % of H_2 was released in the first step of reaction which is driven by a pressure of 0.1 MPa at 30 °C [2].

Nuance of H_2 production involves decomposition mechanism, reaction kinetics, and optimum onset temperature which highly rely on the additives to provoke the process [3]. In order to find out the most suitable candidate among the existing materials, current research is focused on their low temperature performance. Attempts are made to bring out the underlying basic science to improve the (de)hydrogenation capacity [4]. It is imperative to find the reaction enthalpy of H_2 release that controls the onset temperature of H_2 release/uptake in hydrogen storage materials [5].

The dehydriding process is provoked by the instability of the metal hydrides resulting in interim products which should be less reactive to satisfy the mobile energy requirements [6]. Upsetting the stability of parent H_2 absorbant material is a key factor in this aspect [7–9]. Vajo et al. [10,11] have proposed destabilization of LiH and MgH_2 by Si system with an accompanying high gravimetric H_2 release of 9%. However, the high reaction enthalpy hampers the initiation of such a decomposition reaction. For on-board applications [2] the reaction energy of $\leq$ 20–30 (kJ mol^{-1} H_2) along with the hydrogen storage density of more than 6 wt % H_2 are desired. Therefore research is driven to find a suitable material that satisfies the above conditions as well as to understand their reaction energetics. Moreover, knowledge on reaction possibilities by adding different additive is needed. This has motivated us to pursue in this direction.

Adding catalysts is a good contender. For example, the role of MgH_2 as a catalyst when added to $LiBH_4$ [12,13], NbF_5 added to MgH_2 [11], and other such materials [14,16–19], have been investigated. In the case of MgH_2, 7 mol % of the additive NbF_5 and TiF_3 yield fast dehydriding process, whereas for $NaAlH_4$, TiF_3 is better compared to $TiCl_3$ [20]. The transition metal added metal hydrides [21] are found to instigate the decomposition temperature to 40 °C. Moreover, fluorination was shown [14,15] to have a stronger influence on the MgH_2 decomposition process than chlorination as the former reduces the bond strength of the metal hydrides. Since the affinity of transition metal cations toward hydrogen is high [22,23]and Ti exists in its highest valence state of Ti^{4+}, TiF_4 provokes the decomposition mechanism at reduced temperature. Thus, transition metal based catalysts have started to gain prominence.

When TiF_x (x = 4, 3, 2) is added to MgH_2, $Mg(BH_4)_2$, and $Mg(AlH_4)_2$, it plays a dual role: (i) reduces the on-set temperature and (ii) increases the kinetics of hydrogen loading/unloading. Recent studies have heralded that the TiF_4 added metal hydrides help in the efficient (de)hydrogenation process [24,25]. When TiF_4 is added, the kinetics of Mg–H_2 and release of hydrogen (desorption mechanism) take place at reduced temperature [26]. Metal-hydrogen bond energy has been decreased by the catalysts and accordingly the desorption temperature of MgH_2 is reduced. Besides, the prolonged catalytic activity relies on covalent bonding which ensures the binding force necessary for catalytic activity [27]. X-ray photoelectron spectroscopy (XPS) analysis by Jain et al. [24], elucidated the potential importance of Ti^{4+} valence state compared to the lower valence states of titanium fluorides and hydrides which shows better catalytic activity [28–30]. The XPS study [24] further showed that, the enhanced hydrogen production is due to the formation of MgF_2 compound during the decomposition mechanism.

TiF_4 takes precedence over other catalysts because of its lower bond cleavage energy. This underscores the necessity of higher valence states to kindle the reaction mechanism. The influence of TiF_x additive onto the magnesium hydrides for H_2 release have been studied experimentally at different temperatures and pressures [24]. Further the intermediate compounds formed at the particular experimental condition have been studied with the aid of XPS. However, the possible reaction pathways and the reaction energy of TiF derivatives with the host magnesium hydrides have not been studied yet. Owing to the large number of candidates involved and the possibility of various ratios of their compositions, experimental studies alone can not provide reaction pathways. In this perspective, theoretical approach could be helpful in describing the nature of chemical reactions happening between the chemical entities and phase stability.

As a first step toward the direction of understanding reaction possibilities, the intrinsic mechanical strain of the fluoride species of titanium (TiF_x; X = 4,3,2). We have been predicted from quantum mechanical density functional theory (DFT) based studies [31]. This shows the additive TiF_4 could survive the pressure generated by the mild ball milling and the kinetics of H_2 release which involve reasonable application of strain [32]. TiF_4 has significantly softer mechanical properties than the other TiF derivatives.

Though non-toxic TiF_4 has been in vogue for H_2 production [33,34], dentistry [35–37], and in Ti powder producing

Please cite this article as: Jebasty RM, Vidya R, Elucidating reaction equations of TiF_x (x = 4,3,2) catalysts for hydrogen storage applications, International Journal of Hydrogen Energy, https://doi.org/10.1016/j.ijhydene.2019.11.187

industry [38], its fundamental properties are yet to be understood. Hence, DFT is leveraged for extracting atomic scale understanding of the materials, and new strategies to improve their properties are suggested. In addition, we have applied the interface reaction concept in order to explore the sustainable, intermediate reactions. In this work, we have found out the transient species formed during the destabilization of metal hydrides, and their favorable thermodynamic reactions.

Here we focus on the possible decomposition products of TiF_x ($x = 4$, 3, and 2) upon adding to magnesium hydrides namely MgH_2, $Mg(BH_4)_2$, and $Mg(AlH_4)_2$. Further, deep insight into the chemical bond stability and interaction strength of the Ti–F bonds are provided using Crystal Orbital Hamiltonian Population (COHP) analysis. The influence of F on the properties of TiF_x has been studied by extending the charge density investigation to the lower valence states of titanium fluoride.

Methods

Computational details

Quantum mechanics based DFT simulation is performed using the quantum engine Vienna Ab-initio Simulation Package (VASP) [39,40]. The projected-augmented-wave (PAW) method with the Perdew, Burke, and Ernzerhof (PBE) parameterization has been employed to treat the exchange and correlation functional [41]. The plane wave cut-off energy of 550 eV is used with $4 \times 4 \times 2$ Gamma centered Automatic k-point meshes. For TiF_3 and TiF_2, spin-polarization was included in the calculation. The projected Crystal Orbital Hamiltonian Population (pCOHP) has been derived using the program "LOBSTER- Local-Orbital Basis Suite Towards Electronic-structure Reconstruction" [42].

The decomposition reaction has been computed from the "Interface Reactions" tool [43] which utilizes the phase diagram based formulation proposed by Richards et al. [43] to find the reaction pathway. Usually, the phase diagrams depict the set of compounds which are involved in a reaction. The nearest neighboring phases between the host compound and the additive have been extracted from the phase diagram. In this method, the ground state formation energy has been extracted from experimental values available in Kubaschewski [44] or NIST-JANAF thermochemical [45,46] tables. If the experimental formation energy of a material is not listed in the above mentioned tables, the theoretical formation energy reported in the Materials Project database is used instead. In the present study, the reaction pathways are derived based on the phase diagram of quaternary Ti–F–Mg–H, multinary Ti–F–Mg–B–H, and Ti–F–Mg–Al–H systems under controlled conditions. For exploring all possible reaction pathways, the ground state energies of the initial and target materials are calculated by setting the accurate DFT parameters. In addition, the formation energy of all the interim compounds involved in various reactions are also calculated. Thus finding the most feasible reaction pathway is ensured.

Results and discussion

Crystal structure

Titanium tetrafluoride takes orthorhombic symmetry [space group no. 161 (*Pnma*)] with the columnar structure of polymeric fluorine bonds [47]. TiF_4 has three different Ti^{4+} sites, each site is bonded to six F atoms forming corner-sharing TiF_6 octahedra which are tilted with angles ranging from 160 to 171°. There is a spread of Ti–F bond lengths ranging from 1.7 to 2.0 Å [31]. The structural findings show that the three different Ti sites are bonded with twelve inequivalent *F* sites. We have classified the F-site, as F-apical (F_a), F-single-bond geometry (F_s), and F-linear bond geometry (F_l) based on its bonding toward the Ti atom. The apical F_a ions are connected to the single Ti^{4+} sites as do the F_s-sites. The remaining fluorine in the F_l position make three linear bonds by sharing two Ti^{4+} sites as shown in Fig. 1. TiF_3 takes up trigonal rhombohedral structure of space group $R\bar{3}c$ with octahedral coordination. TiF_2 crystallizes in the cubic $Fm\bar{3}m$ space group. It forms hexahedron with eight equivalent *F* atoms. The crystal structures were described in detail in Ref. [31].

Chemical reaction of TiF_x-added-magnesium hydrides

DFT as a source of ground state chemical potential, harnesses fundamental understanding on the ground state properties of materials. It allows one to find possible phases during the (de) hydrogenation process from the ground state chemical potential of the reactants involved. In an effort to improve the theoretical understanding of dehydrogenation reaction, we have delineated reaction equations and the intermediate chemical species that are stable at 0K in Table 2. Earlier, for devising these reaction equations, formation energies of reactants, catalysts, and the final products are calculated and given in Table 1. Here, we are focusing on the reaction possibilities for dehydrogenation mechanism when TiF_x is added to MgH_2, $Mg(BH_4)_2$, and $Mg(AlH_4)_2$. Similar to previous studies [48,49], the calculated weight percentage of H_2 release using the gravimetric density formula is also given.

For the first time, we are reporting the chemical reaction at different molar ratios of TiF_x catalyst with the target materials MgH_2, $Mg(BH_4)_2$, and $Mg(AlH_4)_2$. The calculated theoretical gravimetric density of magnesium hydrides are 7.09%, 12.96%, and 8.51% for MgH_2, $Mg(BH_4)_2$, and $Mg(AlH_4)_2$, respectively. The results are in good agreement with the DFT results generated using the Materials Project database [50]. For the sake of comparing our calculated reaction energies with other published works, it is also given in the units of kJ/mol. The experimental reaction energy concerns the thermodynamic energy at reaction temperature whereas our theoretical values correspond to that at zero kelvin. The positive sign implies the capability of the material to store hydrogen, and the negative sign corresponds to the release of hydrogen.

The reported chemical energy of the studied systems of our interest clearly points out the energy necessary to initiate the dehydrogenation process. For instance, when the additive TiF_x is added, five favorable dehydrogenation pathways have been

Please cite this article as: Jebasty RM, Vidya R, Elucidating reaction equations of TiF_x ($x = 4,3,2$) catalysts for hydrogen storage applications, International Journal of Hydrogen Energy, https://doi.org/10.1016/j.ijhydene.2019.11.187

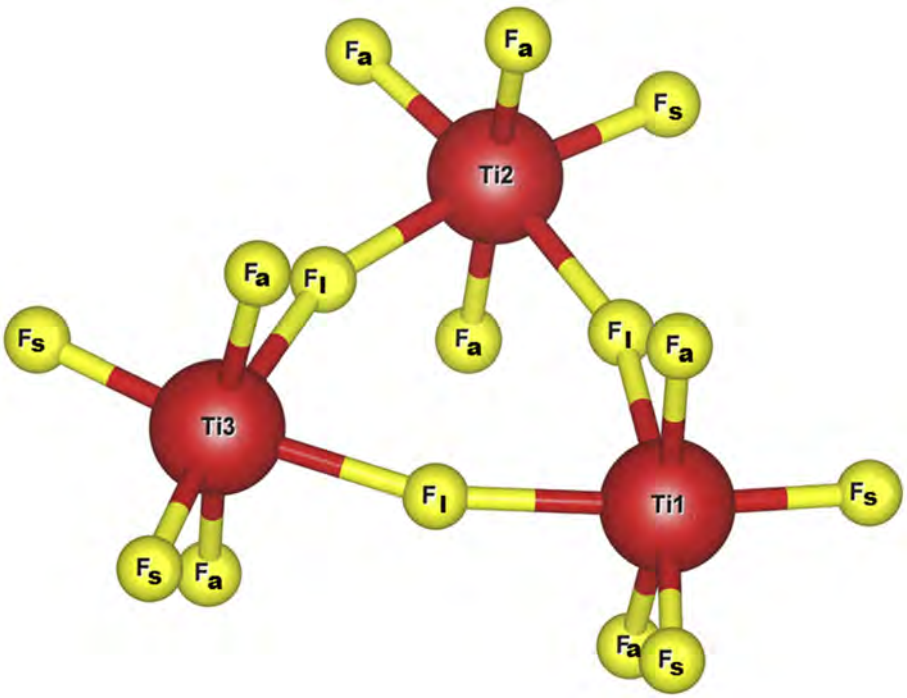

Fig. 1 – Cyclic bonding representation of TiF_4.

observed for MgH_2. When MgH_2 is combined with TiF_4, it readily decomposes into interim products MgF_2, TiH_2 with some release of hydrogen. This may be because ionic bonding in MgH_2[51] is broken and due to electronegativity difference MgH_2 immediately takes up fluorine atoms with the release of hydrogen. Our calculated chemical reaction energetics, Eqns (1)–(3) shows that TiF_4 has better catalytic activity with MgH_2 and helps to form the active species, TiH_2 and MgF_2 (see Eqn. (1)) in agreement with the XPS study(Ref [24]). As per Eqn. (1) for a maximum release of 1.12 wt% of H_2, the reaction energy of −124.3 kJ/mol is required, whereas for 0.73 wt % and 0.50 wt % of H_2 release −110.3 kJ/mol and −32.7 kJ/mol are required (Eqns. (2) and (3)). This implies that TiF_4 has significant role in enabling the reaction process, since the lower valence state additives (TiF_3 and TiF_2) do not help in the release of H_2 considerably.

Table 1 – The formation energy of the compounds involved in the reaction process.

Compound	Formation Energy/atom	
	Present	Ref [50]
$Mg(BH_2)_4$	−0.214	−0.335
$Mg(AlH_2)_4$	−0.013	−0.129
MgH_2	−0.152	−0.276
MgF_2	−3.482	−3.857
$MgTiF_6$	−4.608	−3.821
TiF_4	−3.211	−3.709
TiF_3	−3.269	−3.689
TiF_2	−2.682	−3.022
TiH_2	−0.425	0.584
TiB_2	−1.072	−1.058
TiB	−0.863	−0.832
Ti_3Al	−0.3433	−0.276
Ti_3B_4	−0.270	−0.932
AlF_3	−3.475	−3.891
AlH_3	−0.066	−0.121
BF_3	−2.731	−3.131
BH_3	−0.033	−0.144

When the TiF_x are added to the high gravimetric $Mg(BH_4)_2$, many reaction pathways are possible (see Eqns (6)–(15)). Among the three additives studied, the maximum hydrogen release of 5.44% is obtained for TiF_2 added $Mg(BH_4)_2$ with reaction energy of 80 kJ/mol. However, additional factors like working temperature or pressure are needed for reducing the reaction energy to 30 kJ/mol, in order to make it suitable for on-board applications as per the DoE guidelines. It is notable from the reaction Eqns. 13–15, that due to the endothermic nature of the reaction, storing H_2 in $Mg(BH_4)_2$ is more favorable than its release.

Our calculations show that, TiF_4 added $Mg(BH_4)_2$ has the reaction energy of −5.67 to −143.1 kJ/mol. However, the corresponding energetics from experimental formation energy shows a range of 30–48 kJ/mol [53] which meets the target set by DoE for potential systems. Moreover, experimental studies confirm the improved hydrogen release under 40–90 °C of working temperature [24,25]. It is crucial to mention here that 0.333 M fraction of TiF_4 gives rise to the significant H_2 production of 4.13 wt % from its gravimetric density of 12.96%. In addition, the reversible storage can be facilitated by the metastable by-product BH_3 which further releases hydrogen(Eqns (6)–(9)). This can be a self-driven process since the heat generated by the exothermic reaction may assist in the cleavage of B–H bonds [52]. Therefore, the system $Mg(BH_4)_2$ added with TiF_4 can release high gravimetric H_2. TiF_3 has the same impact as that of TiF_4 when added to $Mg(BH_4)_2$. Though the reaction energy seems to be higher (−105.3 kJ/mol), the

Please cite this article as: Jebasty RM, Vidya R, Elucidating reaction equations of TiF_x (x = 4,3,2) catalysts for hydrogen storage applications, International Journal of Hydrogen Energy, https://doi.org/10.1016/j.ijhydene.2019.11.187

Table 2 – The possible reaction pathways when TiF_x is added to MgH_2, $Mg(BH_4)_2$, and $Mg(AlH_4)_2$ and the energy released during the reaction.

System	Eqn. No.	Reaction equation	E_{rxn} /atom (kJ/mol)	E_{rxn} /atom (eV/atom)	E_{rxn} (eV/atom)	H_2 production
			Present	Present	Ref. [50]	wt. %
TiF_4–MgH_2	1	$0.667\ MgH_2 + 0.333\ TiF_4 \rightarrow 0.333\ TiH_2 + 0.667\ MgF_2 + 0.333\ H_2$	−124.3	−1.293	−1.348	1.12
	2	$0.333\ MgH_2 + 0.667\ TiF_4 \rightarrow 0.667\ TiF_3 + 0.333\ MgF_2 + 0.333\ H_2$	−110.3	−1.148	−1.179	0.73
	3	$0.25\ MgH_2 + 0.75\ TiF_4 \rightarrow 0.25\ MgTiF_6 + 0.5\ TiF_3 + 0.25\ H_2$	−32.7	−0.340	−0.049	0.50
TiF_3–MgH_2	4	$0.600\ MgH_2 + 0.4\ TiF_3 \rightarrow 0.4\ TiH_2 + 0.6\ MgF_2 + 0.2\ H_2$	−82.7	−0.860	−0.907	0.69
TiF_2–MgH_2	5	$0.5\ MgH_2 + 0.5\ TiF_2 \rightarrow 0.5\ TiH_2 + 0.5\ MgF_2$	−51.6	−0.537	−0.572	0.0
	6	$0.667\ Mg(BH_4)_2 + 0.333\ TiF_4 \rightarrow 0.667\ BH_3 + 0.333\ TiB_2 + 1.667\ H_2 + 0.667\ MgF_2$	−143.1	−1.489	−1.562	4.16
TiF_4–$Mg(BH_4)_2$	7	$0.4\ Mg(BH_4)_2 + 0.6\ TiF_4 \rightarrow 0.4\ BH_3 + 0.4\ MgTiF_6 + 0.2\ TiB_2 + H_2$	−5.67	−0.059	−0.562	2.05
TiF_4–$Mg(BH_4)_2$	8	$0.25\ Mg(BH_4)_2 + 0.75\ TiF_4 \rightarrow 0.5\ BH_3 + 0.5\ TiF_3 + 0.25\ MgTiF_6 + 0.25\ H_2$	−32.8	−0.341	−0.063	0.47
	9	$0.1\ Mg(BH_4)_2 + 0.9\ TiF_4 \rightarrow 0.8\ TiF_3 + 0.1\ MgTiF_6 + 0.2\ BF_3 + 0.4\ H_2$	−68.4	−0.711	−0.588	0.85
	10	$0.6\ Mg(BH_4)_2 + 0.4\ TiF_3 \rightarrow 0.4\ BH_3 + 0.4\ TiB_2 + 1.8\ H_2 + 0.6\ MgF_2$	−105.3	−1.095	−1.118	4.64
TiF_3–$Mg(BH_4)_2$	11	$0.333\ Mg(BH_4)_2 + 0.667\ TiF_3 \rightarrow 0.333\ MgTiF_6 + 0.333\ TiB_2 + 1.333\ H_2$	−34.6	−0.360	−0.947	2.95
	12	$0.5\ Mg(BH_4)_2 + 0.5\ TiF_2 \rightarrow 0.5\ TiB_2 + 2\ H_2 + 0.5\ MgF_2$	−79.7	−0.829	−0.779	5.44
	13	$0.071\ Mg(BH_4)_2 + 0.929\ TiF_2 \rightarrow 0.286\ TiH_2 + 0.571\ TiF_3 + 0.071\ TiB_2 + 0.071\ MgF_2$	18.6	0.195	0.209	0.0
TiF_2–$Mg(BH_4)_2$	14	$0.065\ Mg(BH_4)_2 + 0.935\ TiF_3 \rightarrow 0.032\ Ti_3B_4 + 0.258\ TiH_2 + 0.581\ TiF_2 + 0.065\ MgF_2$	26.73	0.278	0.273	0.0
	15	$0.059\ Mg(BH_4)_2 + 0.941\ TiF_2 \rightarrow 0.118\ TiB + 0.235\ TiH_2 + 0.588\ TiF_3 + 0.059\ MgF_2$	19.90	0.207	0.231	0.0
	16	$0.667\ Mg(AlH_4)_2 + 0.333\ TiF_4 \rightarrow 0.333\ TiH_2 + 0.667\ MgF_2 + 0.333\ H_2 + 1.333\ AlH_3$	−141.73	−1.474	−1.607	0.67
	17	$0.333\ Mg(AlH_4)_2 + 0.667\ TiF_4 \rightarrow 0.667\ TiH_2 + 0.333\ MgF_2 + 0.667\ H_2 + 0.667\ AlF_3$	−155.3	−1.615	−1.752	1.19
TiF_4–$Mg(AlH_4)_2$	18	$0.111\ Mg(AlH_4)_2 + 0.889\ TiF_4 \rightarrow 0.889\ TiF_3 + 0.111\ MgF_2 + 0.444\ H_2 + 0.222\ AlF_3$	−118.3	−1.208	−1.259	0.75
	19	$0.1\ Mg(AlH_4)_2 + 0.9\ TiF_4 \rightarrow 0.8\ TiF_3 + 0.1\ MgTiF_6 + 0.2\ AlF_3 + 0.4\ H_2$	−84.5	−0.879	−0.761	0.66
	20	$0.6\ Mg(AlH_4)_2 + 0.4\ TiF_3 \rightarrow 0.4\ TiH_2 + 0.6\ MgF_2 + 0.2\ H_2 + 1.2\ AlH_3$	−98.4	−1.023	−1.14	0.43
TiF_3–$Mg(AlH_4)_2$	21	$0.273\ Mg(AlH_4)_2 + 0.727\ TiF_3 \rightarrow 0.727\ TiH_2 + 0.273\ MgF_2 + 0.364\ H_2 + 0.545\ AlF_3$	−74.3	−0.773	−0.881	1.72
	22	$0.5\ Mg(AlH_4)_2 + 0.5\ TiF_2 \rightarrow 0.5\ TiH_2 + 0.2\ MgF_2 + AlH_3$	35.9	0.373	0.391	0.0
TiF_2–$Mg(AlH_4)_2$	23	$0.2\ Mg(AlH_4)_2 + 0.8\ TiF_2 \rightarrow 0.8\ TiH_2 + 0.2\ MgF_2 + 0.4\ AlF_3$	−33.9	−0.353	−0.351	0.0
	24	$0.034\ Mg(AlH_4)_2 + 0.966\ TiF_2 \rightarrow 0.621\ TiF_3 + 0.069\ Ti_3Al + 0.138\ TiH_2 + 0.034\ MgF_2$	34.7	0.361	0.402	0.0

experimental reaction energy calculated for the products in their standard states is −29.4 kJ/mol corresponding to the 4.64% of H_2 release [53].

Finally, the TiF_x added $Mg(AlH_4)_2$ undergoes the dehydrogenation process when adding TiF_4 and TiF_3. In turn, TiF_2 facilitates hydrogenation similar to the previous case. Further, theoretical hydrogen release of < 2% is observed in the first reaction step when adding all the TiF variants. However, the interim product reversibly stores hydrogen as solid TiH_2.

If we look into the reaction equations from the perspective of DoE system targets, it is clear from Table 1, that the reaction energy is higher for chemical entities MgH_2 and $Mg(AlH_4)_2$ when TiF_x catalyst is added. In the case of $Mg(BH_4)_2$, the minimum energy required for the reaction to occur is −5.67 kJ/mol for the additive TiF_4. However it requires 0.6 mol % of TiF_4 for releasing only 2.05 wt % of H_2. For the same system, still higher H_2 release (4.16%) is observed with 0.33 M fraction of the TiF_4 catalyst along with the experimental reaction energy

Please cite this article as: Jebasty RM, Vidya R, Elucidating reaction equations of TiF_x (x = 4,3,2) catalysts for hydrogen storage applications, International Journal of Hydrogen Energy, https://doi.org/10.1016/j.ijhydene.2019.11.187

of −40 kJ/mol. This is a very promising sign for the mobile energy applications.

In the case of 0.4 mol % TiF_3 added to $Mg(BH_4)_2$, the experimental reaction energy of −29.8 kJ/mol has been observed for 4.64 wt % of H_2 release (given in supplementary file, Fig. 1). Moreover, the hydrogen remains in the system as hydrides when adding TiF_3 which may be released in the subsequent reaction steps. It is interesting to note that when 0.5 mol % of TiF_2 is added to the $Mg(BH_4)_2$ system, it induces greater H_2 production of 5.44 wt % with the experimental reaction energy of −94.9 kJ/mol, compared to TiF_4 and TiF_3. This implies that the reaction may take place only with the aid of any additional variables like temperature or pressure. However, the mixing ratio of the additive should be small so that the gravimetric density of H_2 storage capacity is not affected. Accordingly we could infer that TiF_4 and TiF_3 are better catalysts based on the reaction equations.

Optimistic view of the results show that, the degradation products formed in the case of additive TiF_4 is same as that observed in the experimental XRD peaks [54]. Further, there is no peak corresponding to the TiH_2 compound because of negligible quantity upon reaction with MgH_2. Similar sign of less mol % of TiH_2 is confirmed by our reaction equations. This gives an insight into the dissociation reaction of hydrogen release. It is obvious from Eqns. (5 and 22–24) that H_2 molecule is not released when TiF_2 reacts with MgH_2 and $Mg(AlH_4)_2$. The above results suggest that small molar fraction of TiF_4 is enough to trigger the dehydrogenation process. Regardless of the reaction formation energy value, all equations are feasible except reaction with TiF_2 which has positive energy indicating H_2 storage instead of its release. The maximum extraction of H_2 from $Mg(BH_4)_2$ is achieved for 0.333 mol % of TiF_4, 0.4 mol % of TiF_3 and 0.5 mol % of TiF_2. However, the discussion on intermediate phases which are stable at certain experimental conditions are out of scope of this work.

Density of States and chemical bonding

In a bid to look into the bonding nature of the material, the total and atom projected Density of States (DOS) of TiF_4 are given in Fig. 2. TiF_4 has a fundamental band-gap of 3.9 eV between valence band maximum (VBM) and conduction band minimum (CBM) which implies its transparent nature, in excellent agreement with the previous theoretical report, but less than the experimental value [55]. The degenerate states of Ti and F atoms in the entire energy range in valence band indicate the significant covalent interaction. Further, the DOS from −1 to 0 eV contains the states from F_a, F_l, and F_s atoms. The VBM is mainly contributed by the *p* orbital of F_s and some F_l sites, which readily involve in optical transition. Remarkably, the Fermi level(E_F) is influenced by the F-2*p* states while the conduction band is formed by the states from Ti cation.

The apical fluorine atoms build a linear Ti—F—Ti—F—Ti bond throughout the structure with tilted ∠F—Ti—F angle of ≈ 171° far from that of perfect octahedra. This results in energetically degenerate states of Ti-*d* orbitals and F_a-*p* orbitals in the −4 to −4.5 eV energy range. The states spreading from −3.5 to −3 eV are made up of highly degenerate Ti−3*d* and 2*p* states from F_l atom. This in turn results in strong interaction between these two ions, leading to intense bonding states in the COHP plot as discussed in the next section.

As the partial filling of *d* orbital in TiF_3 and TiF_2 leads to the spin polarization, we have performed spin-polarized calculations which show that the total magnetic moment is 0.97 μ_B, and 1.83 μ_B per formula unit for TiF_3 and TiF_2, respectively. The spin-polarized DOS plot of TiF_3 (Fig. 2b) shows metallic character with finite Ti-*d* electrons at the Fermi level (E_F). TiF_2 has small band gap value of 0.4 eV with unique co-existence of ferromagnetic and insulating behaviour. It may be noted that the band gap value is usually underestimated by DFT. Further studies are needed to explore the possibility of using TiF_2 in dilute magnetic semiconductor applications. Noticeably, the occupancy of the orbital states in TiF_2 is distinct from TiF_4 and TiF_3. Here, both the VBM and CBM are occupied by Ti-*d* states. This strong *d* electron presence in both VBM and CBM could be the reason for the contra-catalytic response of TiF_2 compared to the other two compounds studied here.

COHP analysis

To project the PAW functional onto localized orbital, we have used the bond analytical tool "LOBSTER" [56,57] which is explained in detail elsewhere [58]. In order to quantify the bonding strength, we have calculated the pCOHP for the TiF variants. The integrated COHP value can be considered as a measure of the bond strength. It euphemistically addresses bond energy which corresponds to the bond stability. Higher the ICOHP value more is the stability and vice versa [59]. For a covalent bond, the -ICOHP is maximum when all the bonding orbitals are occupied by electrons. Smaller relative value of -ICOHP indicates more ionic nature of the bond. The energy integral up to E_F denoted by integrated pCOHP value and the corresponding bond-lengths of the interacting atoms are given in Table 3.

Fig. 2c shows that the bonding and anti-bonding states are contributed by negative and positive pCOHP, respectively. The unique bonding arrangement of TiF_4 has been analyzed in detail in Ref. [31]. In this context, bonding interaction pattern is same for all the three Ti^{4+} sites towards their F_l, F_s and F_a neighbors. In order to have more clarity, we have shown the pCOHP plot for the Ti1 site interaction. The COHP curve is dominated by filled states in TiF_4, which in turn leads to covalent bonding. The anti-bonding states are observed in the higher energy region. In addition, the ICOHP values indicate the anisotropic nature of bonding and thus confirm our previous report [31]. For instance, a strong interaction is observed between Ti and F_s sites in the energy range −2 to −1 eV, thereby forming stable bonding states due to the overlapping population which makes it stronger [59]. Hence the interaction of F_s atoms is active in the aforementioned energy range. This yields strong bonding energy of −6.0 eV to the Ti-F_s hybridization.

Further, the bonding states around −3.5 to −3 eV arise due to the influence of F_l sites. This implies a very strong orbital mixing of Ti-*d* with F-*p* orbitals. However, Ti and F_l orbitals have weaker mixing in the 0 to −0.5 eV energy range, implying significant ionic character in their bonding. Also, it is noticeable from DOS (Fig. 2a) that the E_F solely has strong *p* character of F atom. Hence there is no orbital overlapping of Ti and F

Please cite this article as: Jebasty RM, Vidya R, Elucidating reaction equations of TiF_x ($x = 4,3,2$) catalysts for hydrogen storage applications, International Journal of Hydrogen Energy, https://doi.org/10.1016/j.ijhydene.2019.11.187

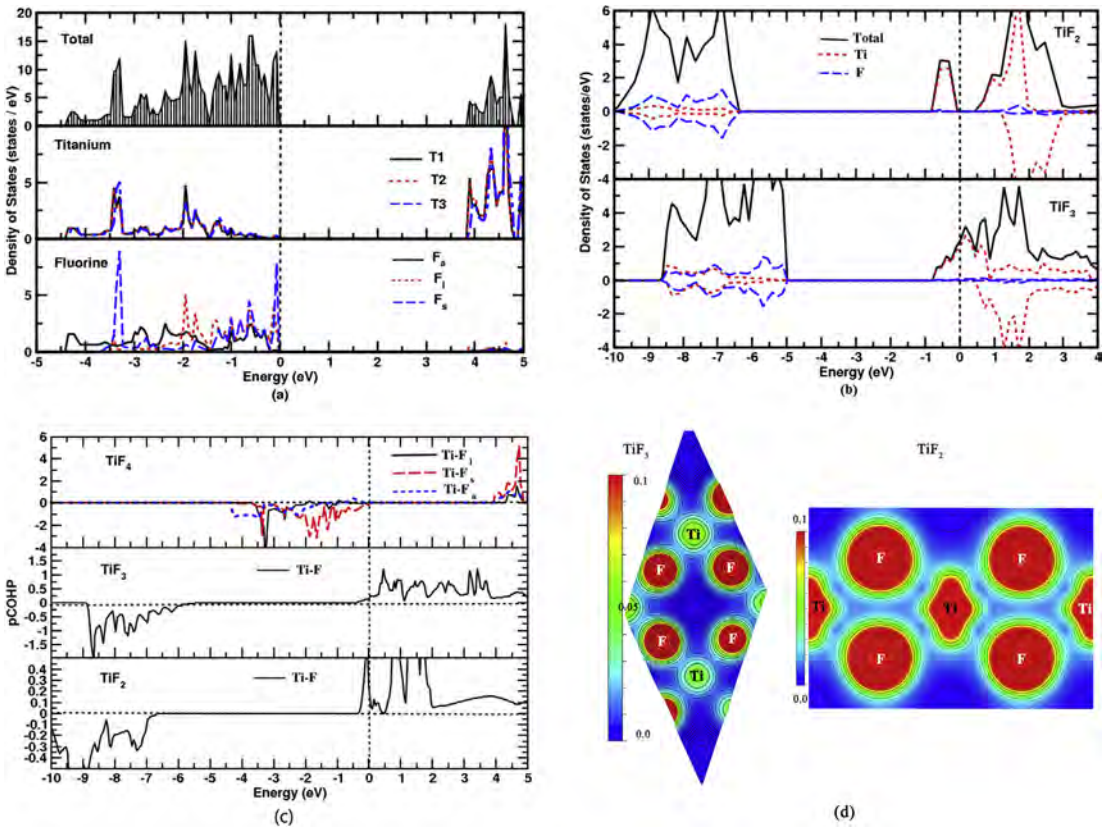

Fig. 2 – (a) Density of States of TiF_4 (b) DOS of TiF_2 and TiF_3 (c) Bond strength of TiF_4, TiF_3 and TiF_2 from COHP analysis (d) Charge density of TiF_3 and TiF_2.

atoms at E_F. Due to orthogonality condition of COHP, overlapping of F-*p* orbital with band function leading to nonbonding states at the E_F. However, low energetic bonding states are visible in the lower valence region and hence results in weak interaction of Ti with F_a atom.

TiF_3 consists of unfilled states called anti-bonding states depleting into the E_F, thus establishing a quasi-meta stable state. For both TiF_3 and TiF_2, a few anti-bonding states cross at E_F reflecting the ionic character of bond. The ionic radius increases upon moving towards lower oxidation states from Ti^{4+} to Ti^{2+} (0.74–1.0 Å), thus making it easier to remove an electron since it is less bound to the nucleus. It is clearly reflected in bond strength of the TiF derivatives. The bond strength value (-ICOHP) follows a decreasing trend as TiF_4 > TiF_3 > TiF_2. Hence the higher valence states can prolong the catalytic activity.

In TiF_4, due to the strong covalent character inside the ring and ionic nature surrounding the ring of octahedral F^- anion [31], the catalytic efficiency might be enhanced. The bonding feature also confirms that the inner fluorine (F_l) counterparts have less bonding energy compared to the fluorine lying outside (F_s) in the triangular cage. This results in short and long Ti–F bonds. This strongly implies that the combination of metal-halogen bonds (Ti-F_l) may readily be involved in interaction with external chemical reaction because of its higher electron density inside the cage. In turn forms strong Ti–H bonds, in the place of Ti–F bonds with the ease to attract hydrogen since the halogen and hydrogen bonds imitate one another. Further, Fig. 2d shows the charge density plot of TiF_3 and TiF_2. TiF_3 shows ionic nature with less covalency, whereas the fluorine in TiF_2 has spherical charge distribution implying ionic bonding. The charge density distribution is well aligned with the above discussed ICOHP values. The low electron density between the Ti and F atoms for both systems results in less affinity with the host metal hydrides. This bonding feature may be the reason for the insignificant catalytic activity of TiF_3 and TiF_2.

Table 3 – Calculated bond strength of TiF derivatives.

Compound	Interaction	Bond distance(Å)	ICOHP
TiF_4	Ti-F_l	2.001	−2.972
	Ti-F_s	1.775	−5.990
	Ti-F_a	1.936	−3.282
TiF_3	Ti–F	1.970	−3.336
TiF_2	Ti–F	2.221	−1.729

Optical properties

Based on the above discussions, even though TiF_4 and TiF_3 have favorable properties we extended our optical property analysis on TiF_4, because TiF_3 is metallic. The dielectric function describes the response of a given material to an external electric field, in particular the imaginary component describes the energy losses which occur in a medium due to electronic transitions and is therefore related to

Please cite this article as: Jebasty RM, Vidya R, Elucidating reaction equations of TiF_x (x = 4,3,2) catalysts for hydrogen storage applications, International Journal of Hydrogen Energy, https://doi.org/10.1016/j.ijhydene.2019.11.187

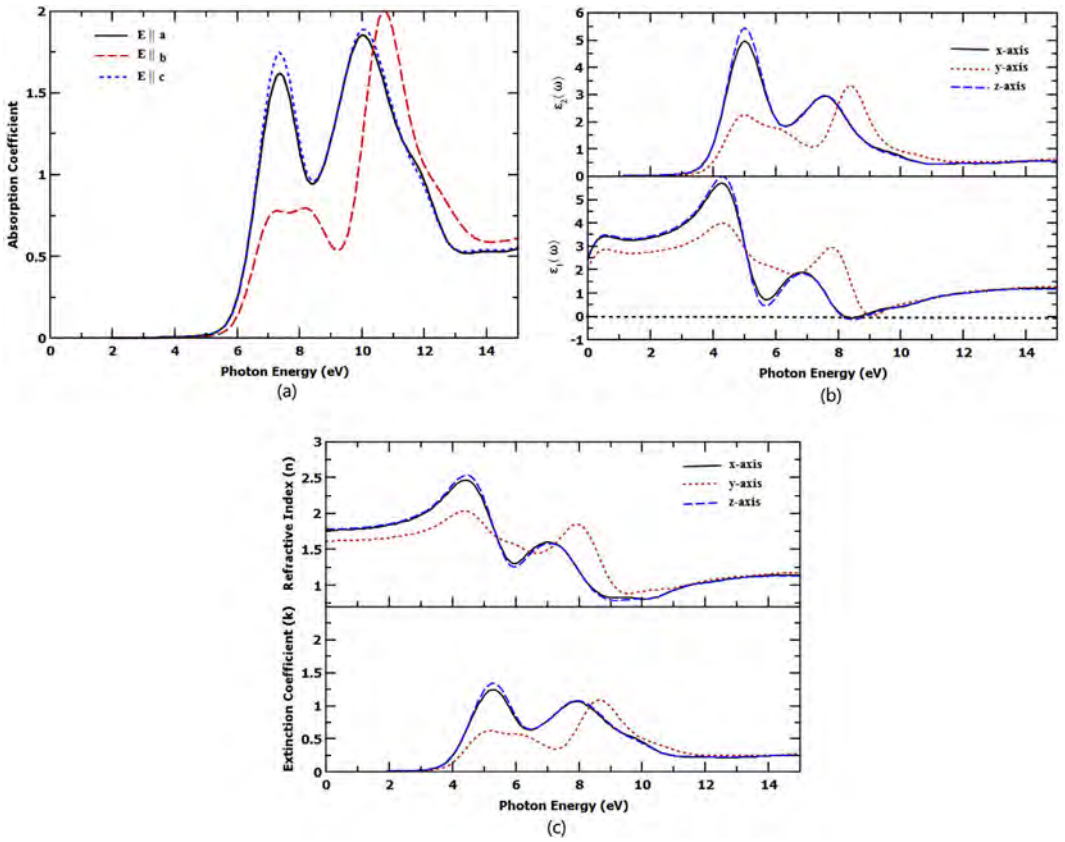

Fig. 3 – (a) Absorption Coefficient (b) Real $\varepsilon_1(\omega)$ and imaginary $\varepsilon_2(\omega)$ part of dielectric constant, and (c) Extinction coefficient, Refractive Index.

absorption [60]. Orthorhombic symmetry produces three non-zero dielectric components for the applied electric field namely $\varepsilon_2(\omega)$. Fig. 3 shows the absorption coefficient derived from the imaginary part of the dielectric function. Herein, Fig. 3a holds absorption spectra, showing the possible transition which is reasonable to discuss, and Fig. 3b, c, representing dielectric functions and the refractive index. The electronic property shows insulating nature matching with the studied metal hydrides MgH_2, $Mg(BH_2)_2$, $Mg(AlH_2)_2$ promoting the positive response compared to the other catalysts.

The absorption spectra, dielectric function, extinction coefficient and refractive index of Ti–F derivatives have been calculated for light polarization parallel and perpendicular to the principle crystallographic axis. TiF_4 has a high dielectric strength and a relatively wide band gap. We observed the maximum absorption peak at 7.4 eV and 10.0 eV for light parallel to the *a* and *c* axis, respectively. For the plane parallel to the *b* axis the maximum absorption at 10.8 eV is followed by the broad absorption peak in the 6.5–8.0 eV energy range. Imaginary part of the dielectric function has a singularity at zero frequency in TiF_3 and thus have optically metallic property(not shown). TiF_4 shows two prominent peaks at about 5 and 7.5 eV for E || *a*, *c* while in E || *b* the second peak is shifted to the right by 1 eV.

Further the electronic structure confirms the optical transition from F-2*p* states to Ti-3*d* states which form the Ti–F optical channel. The valence band maximum is contributed by the orbitals of the F_s sites (F4 and F8 ions) and the minimum of conduction band consists of Ti3-d_{xy}, Ti3-d_{zx} orbitals, thereby electronic excitations involve transition to the Ti3-d_{xy} state.

The real part of the dielectric function of TiF_4 is plotted in Fig. 3b. Value of static dielectric constant (value of dielectric function at zero energy) in case of E || *a* and *c* is 2.5 while for E || *b* is 2.0. Also the refractive index along *a* and *b* axis is 1.75 whereas for the *b*-axis is 1.6 and the corresponding relative dielectric constant (from the relation $\varepsilon = n^2$) is 3.06 and 2.56, respectively. The absorption decreases and thus the corresponding refractive index, shows direct proportion. The refractive index *n* for Fluoroapatite, Chloroapatite and Bromoapatite are 1.17, 1.19 and 1.21, respectively [61]. In a way, the refractive index of TiF_4 suggests that, it is close to that of tooth mineral Hydroxyapatite (1.65). Hence TiF_4 can be used as a dental filling material since it has the desired aesthetics. It may be recalled that we have shown in Ref. [31] that the TiF_4 has the required mechanical stability too.

Conclusions and outlook

Using the chemical energy obtained from the DFT calculation, the ability of the "Interface reaction" tool in elucidating the desorption mechanism of hydrogen storage materials for the conventional magnesium hydrides are studied for the bench marking calculations. We systematically investigated the

Please cite this article as: Jebasty RM, Vidya R, Elucidating reaction equations of TiF_x ($x = 4,3,2$) catalysts for hydrogen storage applications, International Journal of Hydrogen Energy, https://doi.org/10.1016/j.ijhydene.2019.11.187

effect of titanium fluoride compounds on the de/hydrogenation reaction of prominent metal hydrides. Present study is focusing on the reaction energy and chemical bonding of TiF_x ($x = 4, 3, 2$) when added to MgH_2, $Mg(BH_4)_2$, and $Mg(AlH_4)_2$. The difference in energy between the bond-breaking and bond-forming processes determines whether a chemical reaction is exothermic or endothermic. Surprisingly, the catalyst TiF_4 and TiF_3 induce the reaction at energy of less than 40 kJ/mol along with 4.64 wt % of H_2 release, which meets the system targets set by DoE for the year 2020. Herein, TiF_x involves in the reaction process and stabilizes the intermediate compounds also. So, we have provided basic understanding in this aspect. The overall reaction equations show that the process of H_2 release is easier, when the additive contains higher oxidation state of Ti. The charge density analysis shows that TiF_4 has significant iono-covalent bonds providing asymmetrical electron cloud in the Ti–F lattice. This plays an important role in reducing the reaction energy barrier resulting in the enhanced catalytic response.

The bonding analysis and complex dielectric function are explored for TiF_4 to explain its fascinating role as a catalyst. The range of ICOHP values for various Ti–F bonds emphasizes the iono-covalent character of bonds in TiF_4. The high bonding strength derived from ICOHP values indicate dominant covalent characteristic of the bonds between Ti and F atoms which can lead to the sustainable catalytic activity of TiF_4. The origin of its high hardness value has been explained with the aid of COHP plot. The wide band-gap and refractive index value similar to that of hydroxy-apatite provide a hint for its aesthetic appearance when used as a dental-filling material. We have already shown that TiF_4 has the required hardness values for applications in dentistry. The unique bonding arrangements which construct polyhedral cages in TiF_4 are shown to cause exotic properties. Our results will hopefully motivate further studies in the respective systems.

Using the interface reaction tool, a great deal of information has been extracted. As mentioned earlier, owing to large number of candidates, it is essential to elicit the advanced materials which are suitable for mobile energy application. So, the tool can be effectively utilized to identify suitable hydrogen storage material, by shortlisting the aspirants based on the reaction energy as well as the H_2 release. Further the chemical hydrides which are the intermediate products of the reactions can also be examined for their ability to release H_2.

Acknowledgements

The author R. Mariyal Jebasty is grateful to Centre for Research, Anna University, Chennai for offering Anna Centenary Research Fellowship (Lr. No. CFR/ACRF/2017/41). The authors are grateful to DST-SERB, India for the funding under sanction SB/FTP/PS-009/2014 availed for the computer facilities.

Appendix A. Supplementary data

Supplementary data to this article can be found online at https://doi.org/10.1016/j.ijhydene.2019.11.187.

REFERENCES

[1] Department of Energy- Hydrogen storage system Target. https://www.energy.gov/eere/fuelcells/hydrogen-storage.
[2] Dornheim M. Thermodynamics of metal hydrides: tailoring reaction enthalpies of hydrogen storage materials. In: Thermodynamics-Interaction Studies-Solids. IntechOpen: Liquids and Gases; 2011. https://doi.org/10.5772/21662.
[3] Nomura K, Akiba E, Ono S. Kinetics of the reaction between Mg_2Ni and hydrogen. Int J Hydrogen Energy 1981;6(3):295–303.
[4] Holtz R, Imam M. Hydrogen storage characteristics of ball-milled Magnesium-Nickel and Magnesium-Iron alloys. J Mater Sci 1999;34(11):2655–63.
[5] Song M, Kwon S, Mumm DR, Hong S-H. Development of Mg-Oxide–Ni hydrogen-storage alloys by reactive mechanical grinding. Int J Hydrogen Energy 2007;32(16):3921–8.
[6] Malka I, Czujko T, Bystrzycki J. Catalytic effect of halide additives ball milled with magnesium hydride. Int J Hydrogen Energy 2010;35(4):1706–12.
[7] Corno M, Pinatel E, Ugliengo P, Baricco M. A computational study on the effect of fluorine substitution in $LiBH_4$. J Alloy Comp 2011;509:S679–83.
[8] Kou H, Xiao X, Li J, Li S, Ge H, Wang Q, Chen L. Effects of fluoride additives on dehydrogenation behaviors of $2LiBH_4$+MgH_2 system. Int J Hydrogen Energy 2012;37(1):1021–6.
[9] Saldan I, Campesi R, Zavorotynska O, Spoto G, Baricco M, Arendarska A, Taube K, Dornheim M. Enhanced hydrogen uptake/release in 2LiH–MgB_2 composite with titanium additives. Int J Hydrogen Energy 2012;37(2):1604–12.
[10] Vajo JJ, Mertens F, Ahn CC, Bowman RC, Fultz B. Altering hydrogen storage properties by hydride destabilization through alloy formation: LiH and MgH_2 destabilized with Si. J Phys Chem B 2004;108(37):13977–83.
[11] Vajo JJ, Skeith SL, Mertens F. Reversible storage of hydrogen in destabilized $LiBH_4$. J Phys Chem B 2005;109(9):3719–22.
[12] Bösenberg U, Kim JW, Gosslar D, Eigen N, Jensen TR, Von Colbe JB, Zhou Y, Dahms M, Kim D, Günther R, et al. Role of additives in $LiBH_4$–MgH_2 reactive hydride composites for sorption kinetics. Acta Mater 2010;58(9):3381–9.
[13] Barkhordarian G, Klassen T, Dornheim M, Bormann R. Unexpected kinetic effect of MgB_2 in reactive hydride composites containing complex borohydrides. J Alloy Comp 2007;440(1–2):L18–21.
[14] Malka I, Pisarek M, Czujko T, Bystrzycki J. A study of the ZrF_4, NbF_5, TaF_5, and $TiCl_3$ influences on the MgH_2 sorption properties. Int J Hydrogen Energy 2011;36(20):12909–17.
[15] Jin S-A, Shim J-H, Cho YW, Yi K-W. Dehydrogenation and hydrogenation characteristics of mgh2 with transition metal fluorides. J Power Sources 2007;172(2):859–62.
[16] Wang P, Kang XD, Cheng HM. Improved hydrogen storage of TiF_3-doped $NaAlH_4$. ChemPhysChem 2005;6(12):2488–91.
[17] Suib SL. New and future developments in catalysis: batteries. In: Hydrogen storage and fuel cells. Newnes; 2013.
[18] Puszkiel JA. Tailoring the kinetic behavior of hydride forming materials for hydrogen storage. In: Gold nanoparticles-reaching new heights. IntechOpen; 2018.
[19] Abe J, Ajenifuja E, Popoola O. Hydrogen energy, economy and storage: review and recommendation. Int J Energy Res 2019;44(29):15072–86.
[20] Ma L-P, Kang X-D, Dai H-B, Liang Y, Fang Z-Z, Wang P-J, Wang P, Cheng H-M. Superior catalytic effect of TiF_3 over $TiCl_3$ in improving the hydrogen sorption kinetics of MgH_2: catalytic role of fluorine anion. Acta Mater 2009;57(7):2250–8.

Please cite this article as: Jebasty RM, Vidya R, Elucidating reaction equations of TiF_x ($x = 4,3,2$) catalysts for hydrogen storage applications, International Journal of Hydrogen Energy, https://doi.org/10.1016/j.ijhydene.2019.11.187

[21] Ismail M, Mustafa N, Juahir N, Yap FH. Catalytic effect of $CeCl_3$ on the hydrogen storage properties of MgH_2. Mater Chem Phys 2016;170:77–82.
[22] Deledda S, Borissova A, Poinsignon C, Botta W, Dornheim M, Klassen T. H-sorption in MgH_2 nanocomposites containing Fe or Ni with fluorine. J Alloy Comp 2005;404:409–12.
[23] De Castro J, Yavari A, LeMoulec A, Ishikawa T, et al. Improving H-sorption in MgH_2 powders by addition of nanoparticles of transition metal fluoride catalysts and mechanical alloying. J Alloy Comp 2005;389(1–2):270–4.
[24] Jain A, Agarwal S, Kumar S, Yamaguchi S, Miyaoka H, Kojima Y, Ichikawa T. How does TiF_4 affect the decomposition of MgH_2 and its complex variants?—an XPS investigation. J Mater Chem A 2017;5(30):15543–51.
[25] Jangir M, Jain A, Agarwal S, Zhang T, Kumar S, Selvaraj S, Ichikawa T, Jain I. The enhanced de/re-hydrogenation performance of MgH_2 with TiH_2 additive. Int J Energy Res 2018;42(3):1139–47.
[26] Zhang X, Ren Z, Zhang X, Gao M, Pan H, Liu Y. Triggering highly stable catalytic activity of metallic titanium for hydrogen storage in naalh 4 by preparing ultrafine nanoparticles. J Mater Chem 2019;7(9):4651–9.
[27] Ma D, Wang Y, Liu A, Li S, Lu C, Chen C. Covalent organic frameworks: promising materials as heterogeneous catalysts for C-C bond formations. Catalysts 2018;8(9):404.
[28] Pilvi T, Ritala M, Leskelä M, Bischoff M, Kaiser U, Kaiser N. Atomic layer deposition process with TiF_4 as a precursor for depositing metal fluoride thin films. Appl Opt 2008;47(13):C271–4.
[29] Grzech A, Lafont U, Magusin PC, Mulder FM. Microscopic study of TiF_3 as hydrogen storage catalyst for MgH_2. J Phys Chem C 2012;116(49):26027–35.
[30] Ren C, Fang ZZ, Zhou C, Lu J, Ren Y, Zhang X, Luo X. In situ X-ray diffraction study of dehydrogenation of MgH_2 with Ti-based additives. Int J Hydrogen Energy 2014;39(11):5868–73.
[31] Jebasty RM, Vidya R. Mechanical properties of multifunctional TiF_4 from first-principles calculations. ACS Biomater Sci Eng 2019;5(4):2001–12.
[32] Hlova IZ, Castle A, Goldston JF, Gupta S, Prost T, Kobayashi T, Chumbley LS, Pruski M, Pecharsky VK. Solvent-and catalyst-free mechanochemical synthesis of alkali metal monohydrides. J Mater Chem A 2016;4(31):12188–96.
[33] Rulis P, Ouyang L, Ching W. Electronic structure and bonding in calcium apatite crystals: Hydroxyapatite, Fluorapatite, Chlorapatite, and Bromapatite. Phys Rev B 2004;70(15):155104.
[34] Thiangviriya S, Plerdsranoy P, Sitthiwet C, Dansirima P, Thongtan P, Eiamlamai P, Utke O, Utke R. MgH_2-TiF_4-MWCNTs based hydrogen storage tank with central tube heat exchanger. Int J Hydrogen Energy 2019;44(36):20173–82.
[35] Torres GB, da Silva TM, Basting RT, Bridi EC, França FMG, Turssi CP, do Amaral FLB, de Paiva Gonçalves SE, Basting RT. Resin-dentin bond stability and physical characterization of a two-step self-etching adhesive system associated with TiF_4. Dent Mater 2017;33(10):1157–70.
[36] M. I. D. d. Medeiros, H. L. Carlo, R. Lacerda-Santos, F. B. d. SOUSA, J. A. RODRIGUES, F. G. d. CARVALHO, et al., Thickness and nanomechanical properties of protective layer formed by TiF_4 varnish on enamel after erosion, Braz Oral Res, 30 (1).
[37] Kandanuru V, Madhusudhana K, Ramachandruni VK, Vitta HM, Babu L. Comparative evaluation of microhardness of dentin treated with 4% titanium tetrafluoride and 1.23% acidic phosphate fluoride gel before and after exposure to acidic PH: an ex vivo study. J Comput Dyn 2016;19(6):560.
[38] Gordon TR, Cargnello M, Paik T, Mangolini F, Weber RT, Fornasiero P, Murray CB. Nonaqueous synthesis of TiO_2 nanocrystals using TiF_4 to engineer morphology, oxygen vacancy concentration, and photocatalytic activity. J Am Chem Soc 2012;134(15):6751–61.
[39] Kresse G, Hafner J. Ab initio molecular dynamics for liquid metals. Phys Rev B 1993;47(1):558.
[40] Kresse G, Joubert D. From ultrasoft pseudopotentials to the projector augmented-wave method. Phys Rev B 1999;59(3):1758.
[41] Perdew J, Burke K, Ernzerhof M. Phys Rev Lett, 77: 3865, Errata. Phys Rev Lett 1997;78(1996):1396.
[42] Dronskowski R, Blöchl PE. Crystal Orbital Hamilton Populations (COHP): energy-resolved visualization of chemical bonding in solids based on density-functional calculations. J Phys Chem 1993;97(33):8617–24.
[43] Richards WD, Miara LJ, Wang Y, Kim JC, Ceder G. Interface stability in solid-state batteries. Chem Mater 2015;28(1):266–73.
[44] Kubaschewski O, Alcock CB, Spencer P. Materials thermochemistry. revised. Oxford OX 3 0 BW, UK: Pergamon Press Ltd, Headington Hill Hall; 1993. p. 363.
[45] Lemmon E, McLinden M, Friend D. Thermophysical properties of fluid systems in NIST chemistry webbook, NIST standard reference database number 69, eds., 20899. 2012.
[46] N.-J. T. Tables, ed. by mw chase, jr, J. Phys. Chem. Ref. Data.
[47] Bialowons H, Müller M, Müller B. Titantetrafluorid—eine überraschend einfache kolumnarstruktur. Anorg Allg Chem 1995;621(7):1227–31.
[48] Ma L-P, Wang P, Cheng H-M. Hydrogen sorption kinetics of MgH_2 catalyzed with Titanium compounds. Int J Hydrogen Energy 2010;35(7):3046–50.
[49] Sakintuna B, Lamari-Darkrim F, Hirscher M. Metal hydride materials for solid hydrogen storage: a review. Int J Hydrogen Energy 2007;32(9):1121–40.
[50] Jain A, Ong SP, Hautier G, Chen W, Richards WD, Dacek S, Cholia S, Gunter D, Skinner D, Ceder G, et al. Commentary: the materials project: a materials genome approach to accelerating materials innovation. Apl Mater 2013;1(1):011002.
[51] Vajeeston P, Ravindran P, Hauback B, Fjellvåg H, Kjekshus A, Furuseth S, Hanfland M. Structural stability and pressure-induced phase transitions in MgH_2. Phys Rev B 2006;73(22):224102.
[52] Lyu J, Lider A, Kudiiarov V. Using ball milling for modification of the hydrogenation/dehydrogenation process in magnesium-based hydrogen storage materials: an overview. Metals 2019;9(7):768.
[53] Richards WD, Miara LJ, Wang Y, Kim JC, Ceder G. https://materialsproject.org/apps/interfacereactions.
[54] Jangir M, Jain A, Yamaguchi S, Ichikawa T, Lal C, Jain I. Catalytic effect of TiF_4 in improving hydrogen storage properties of MgH_2. Int J Hydrogen Energy 2016;41(32):14178–83.
[55] Rocquefelte X, Goubin F, Montardi Y, Viadere N, Demourgues A, Tressaud A, Whangbo M-H, Jobic S. Analysis of the refractive indices of TiO_2, $TiOF_2$, and TiF_4: concept of optical channel as a guide to understand and design optical materials. Inorg Chem 2005;44(10):3589–93.
[56] Armbrüster M, Schnelle W, Schwarz U, Grin Y. Chemical bonding in $TiSb_2$ and VSb_2: a quantum chemical and experimental study. Inorg Chem 2007;46(16):6319–28.
[57] Landrum GA, Dronskowski R. The orbital origins of magnetism: from atoms to molecules to ferromagnetic alloys. Angew Chem Int Ed 2000;39(9):1560–85.
[58] Maintz S, Deringer VL, Tchougréeff AL, Dronskowski R. Lobster: a tool to extract chemical bonding from plane-wave based DFT. J Comput Chem 2016;37(11):1030–5.
[59] Kishore MA, Okamoto H, Patra L, Vidya R, Sjåstad AO, Fjellvåg H, Ravindran P. Theoretical and experimental investigation on structural, electronic and magnetic

Please cite this article as: Jebasty RM, Vidya R, Elucidating reaction equations of TiF_x ($x = 4,3,2$) catalysts for hydrogen storage applications, International Journal of Hydrogen Energy, https://doi.org/10.1016/j.ijhydene.2019.11.187

properties of layered Mn_5O_8. Phys Chem Chem Phys 2016;18(40):27885–96.
[60] Ravindran P, Delin A, Ahuja R, Johansson B, Auluck S, Wills J, Eriksson O. Optical properties of monoclinic SnI^2 from relativistic first-principles theory. Phys Rev B 1997;56(11):6851.
[61] Ptáček P. Identification, characterization and properties of apatites. apatites and their synthetic analogues: synthesis, structure, properties and applications, 111; 2016. 10.5772/62212.

Please cite this article as: Jebasty RM, Vidya R, Elucidating reaction equations of TiF_x ($x = 4,3,2$) catalysts for hydrogen storage applications, International Journal of Hydrogen Energy, https://doi.org/10.1016/j.ijhydene.2019.11.187